Optimization of Energy Harvesting

Mr. S. NAGAKALYAN
Assistant Professor In Mechanical Engg. Department
Gitam University,
Hyderabad Campus,India

Dr. B. RAGHU KUMAR
Professor In Mechanical Engineering Department
K. L. University
Vijayawada, India.

Abstract: **Micro-generators produce electrical energy when subjected to acceleration. Three architectures of inertial micro-generator were identified as suitable for implementation using MEMS technology. Two of these architectures, both resonant in nature, have been reported in the existing literature. The third, a non-resonant type, is new. The architectures have been analyzed and compared within a common framework, based on sinusoidal driving signals and a common set of normalization factors. A simple procedure for the design process of micro-generators was established. Within the analytical framework, the non-resonant generator achieved the highest power density of the three architectures when powered from large amplitude motion, making it the most suitable for powering implanted medical devices.**
Keywords: MATLab, Comsol multi physics software, and CDRG, VDPG, CFPG.

I. INTRODUCTION

Generally Micro-generator does not present any measure of how effectively they perform their intended duty. The most important performance metric for a micro generator is the fraction of the maximum possible output power that is achieved by the generator for the given device volume and vibration source from which the device is powered. In this work, this performance measure is introduced in detail and referred to as the *effectiveness* of the generator. Achieving the highest possible effectiveness is important in order to enable as much Functionality as possible for WSN motes within a given volume.

A general and unified analytical framework for micro-generator devices has not previously been reported in the literature and consequently there is no established method by which to calculate the effectiveness of an inertial micro-generator. This work develops such a unified framework for micro-generator devices and allows the effectiveness to be calculated by specifying distinct classes, or architectures, of inertial generator for which general rules have been established. The definition of these architectures enables the optimality of a generator to be determined over a range of operating parameters and provides a methodology for designing optimized generators for particular applications. Practical constraints on MEMS implementations are also considered and the sensitivity of the different architectures of generator to changes in the operating parameters is investigated.

II. GENERIC INERTIAL GENERATOR MODEL

These definitions are central to the development of the analysis which follows.

Any inertial generator consists of a proof mass, *m*, moving within a volume constrained by a frame. The operating principle is that the inertia of the mass causes it to move relative to the frame when the frame experiences acceleration. This relative displacement can then be used to generate energy by causing work to be done against a damping force, $f(\dot{z})$, which can be realized by extracting energy via an electric or magnetic field or by straining a piezoelectric material. The mass is attached to the frame by a suspension which may be designed solely to constrain the motion of the mass or to also create a resonant mass-spring system of resonant frequency ω_n.

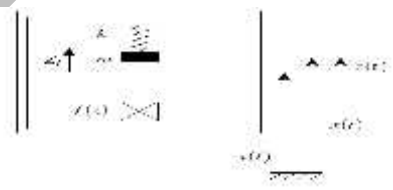

Fig.1: Generic Model of Inertial Generator.

The displacement of the mass from its rest position relative to the frame is denoted as $z(t)$. The absolute motion of the frame is $y(t)$ and that of the proof mass is $x(t) = y(t)+z(t)$. In order to achieve closed form solutions, the driving motion is considered to be a simple harmonic motion, that is, $y(t) = Y_0 \cos\omega t$, where Y_0 is the source motion amplitude. Similarly, Z_0 is the amplitude of the mass-to-frame displacement. In a particular operating case, Z_0 will be mechanically constrained by the Construction of the device. Z_l is defined as a maximum possible Z_0 for a particular device. A generic model of a vibration-driven generator is shown in Figure.1. This is a generalization of the model first presented by Williams, in that the damping force can be realized as any function of the relative velocity between the mass and the frame. The

damping energy per cycle is given by the integral of the damper force with respect to the distance over one cycle of damper movement during a cycle. The actual amount of energy converted from a kinetic form to an electrical form by the damper is less than this and dependent upon the damper's efficiency. For a given mechanical input to the system, this integral is dependent upon the following parameters:

- The proof mass
- The value and characteristic of the damping force
- The displacement limit
- The suspension spring if any (normally expressed in terms of the resonant frequency)

Possible variations in these parameters allow four main classes, or architectures, of generator to be defined based upon different types of damping force and the differing suspension characteristics of the device. There are also different operating modes for the devices. The rest of this work considers three of the four possible architectures in detail. The fourth architecture is shown to be ineffective with current or foreseeable technology and thus is not analyzed in detail.

2.1 Methodology

There are two distinct topologies of an inertial generator. In this thesis these are given the following definitions:

- Resonant topology: the proof-mass is suspended on a spring and resonant energy exchange occurs between mass and spring. As will be shown, to achieve the highest possible power density, the resonant frequency of the mass-spring system should be tuned to the frequency of the driving motion.
- Parametric topology: the suspension does not employ a spring, (or the spring is negligible) and no resonant energy transfers occur.

Two resonant and two parametric generator topologies are considered which leads to the four main architectures of generator. Of the resonant type, one is damped by a force which is proportional to velocity, the velocity-damped resonant-generator (VDRG), and the other is damped by a constant force, the Coulomb-damped resonant-generator (CDRG). One non-resonant and non-linear generator, the Coulomb-force parametric-generator (CFPG) is considered. Variations of VDRGs and CDRGs have been reported previously in the literature. Broadly speaking, the electromagnetic and piezoelectric devices correspond to VDRGs, and the electrostatic devices correspond to CDRGs, although there are exceptions. The CFPG uses a different operating scheme to the others and this will be described later. Other than the work arising from this project, no CFPGs have been reported in the literature. The final architecture possible with these combinations of damping force and generator topology is the velocity-damped parametric generator (VDPG).This generator is shown to be ineffective with current implementation technology and is not investigated further. During this work, the resonant generators were considered to operate in modes in which the proof-mass did not strike the end-stop limits, *i.e.*

$-Z_l<y(t)<Z_l$, and thus the only forces which act on the mass are the inertial, spring and damping forces and gravity. Operating modes in which the mass strikes the end-stop limits were originally excluded because it was thought that the energy dissipated in the collision would reduce the efficiency of the device. It is possible, however, that this operating mode should be considered. It will be shown that for idealized cases of the three architectures considered, the optimal output power can always be derived as a function of $Z_l/Y_0$and ω/ω_n and can be normalized to $Y_0^2\omega^3 m$.Expressions have been normalized using these values so that the plots are general to all Also, Operating conditions for the generators. By normalizing to this common base, fair comparisons between generators can be made, independent of generator size and operating condition. The specific normalization of $Y_0^2\omega^3 m$is used because it has dimensions of power and because a fraction of the maximum kinetic energy of the mass is dissipated in the damper each cycle. The maximum kinetic energy of the mass is proportional to $Y_0^2\omega^2 m$. When this kinetic energy is multiplied by angular frequency (to give a quantity proportional to power) it can be seen that the generator power output is proportional to $Y_0^2\omega^3 m$.

The overall aim of the analysis in this work is therefore two-fold:

- To plot a surface on the normalized axes shown in Figure.2 to show, under different values of the normalized operating conditions of $Z_l/Y_0$and ω/ω_n how much power can be generated by each generator architecture and to compare the power output from each of the architectures.
- To define a quantity referred to as *generator effectiveness* and compare the effectiveness values of reported generators. There are two reasons why an inertial-generator may not generate as much useful electrical energy as is possible within a given volume. The energy dissipated in the damper (which is the energy converted into an electrical form) may not be as large as possible because, as an example, the resonant frequency of the generator may not be tuned to the source vibration. This missed

opportunity in energy dissipation in the damper is not related to an electrical energy loss (as heat, for example) and it is therefore not appropriate to discuss efficiency for the damper. The energy converted in the generator's damper as a fraction of the maximum energy that could be converted in the damper is therefore referred to as the *generator coupling effectiveness*. The second possible reason for a lower output than that which can theoretically be achieved is that some electrical energy may be dissipated as heat in the power processing, or used to control the generator itself. The fraction of the energy dissipated in the damper that is available as useful energy output is referred to as the *generator efficiency*. The *generator effectiveness* is the product of these two terms and is discussed in more detail in Subsection 8.For the cases where the required information was available, table.1,2, and 3(presented at the end) show the effectiveness values for generators reported.

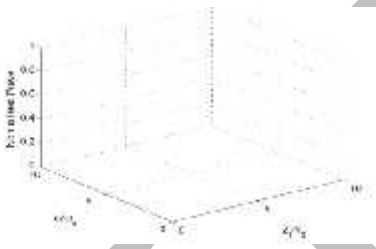

Fig.2 Desired normalized axes to show generator power output.

III. VELOCITY-DAMPED RESONANT GENERATORS

3.1 Ideal Case

A simple mechanical model of a velocity-damped resonant generator (VDRG) is shown in Figure.3, where energy is extracted by a damper whose force is proportional to $\dot{z}(t)$ with a constant of proportionality *D*. As a starting point, an idealized mass-spring system will be analyzed in which the damper represents the energy extraction mechanism. A VDRG can be implemented with an electromagnetic transducer, driving a resistive load, because the damping force in that transducer is proportional to the generated current, which for a resistive load is proportional to the generated EMF. This EMF is in turn proportional to the relative velocity between the mass and frame, and thus the damping force is proportional to the relative velocity

between the mass and the frame. A possible MEMS implementation of a VDRG as shown in Figure.4 and consists of two bonded silicon wafers. The lower wafer has a deposited coil and an etched well in which the mass can move. The upper wafer has a deposited membrane layer and an electroplated magnetic mass. The silicon is etched through to the membrane forming a spring.

The differential equation for the motion of the mass, *m*, relative to the frame is given by:

$$m\ddot{z}(t) = -kz(t) - D\dot{z}(t) - m\ddot{y}(t) \qquad (1)$$

Where k is the spring constant. Taking the Laplace transform of (eq.1) and substituting in expressions for the normalized damping factor, $\zeta = D/2m\omega n$, and the resonant frequency, $\omega n = \sqrt{k/m}$, the transfer function from frame motion, Y(s), to the relative mass-to-frame motion, Z(S) is obtained:

$$\frac{Z(s)}{Y(s)} = \frac{s^2}{s^2 + 2\zeta\omega_n + \omega_n^2} \qquad (2)$$

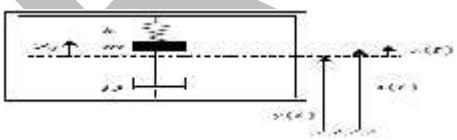

Fig.3 Model of velocity-damped resonant generator.

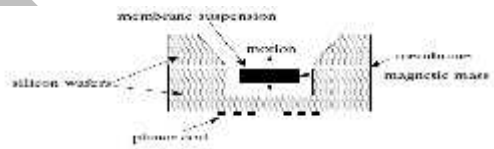

Fig.4 Possible MEMS implementation of VDRG .

The magnitude of the relative motion versus frequency is thus:

$$\frac{z_o}{y_o} = \frac{\omega_c^2}{\sqrt{(1-\omega_c^2)^2 + (2\zeta\omega_c)^2}} \qquad (3)$$

Where $\omega_c = \frac{\omega}{\omega_n}$.

The energy dissipated per cycle is simply the distance integral of the damping force, $D\dot{z}$, over a full cycle:

$$\text{Energy per cycle} = 2D\int_{z=-z_o}^{z_o} \dot{z}\,dz \qquad (4)$$

Calculating this integral for the magnitude of given z_o by (2.3), and multiplying by frequency, gives an expression for the dissipated power.

$$P = \frac{\zeta\omega_c^3 Y_o^2 \omega^3 m}{(1-\omega^2)^2 + (2\zeta\omega_c)^2} \qquad (5)$$

This suggests that for $\omega_c = 1$, the power extracted can be increased without limit by decreasing ζ.

This occurs because:

- The source motion has been assumed unconstrained, *i.e.* it is capable of supplying infinite power.
- There is no limit on Z_o, so at $\omega_c = 1, Z_o \to \infty$ for $\zeta \to 0$.
- There is no parasitic damping present in the system.

All three of these factors will be addressed in section eq.7 to show what can be achieved from practical generators operating at the resonant frequency. Building on the previous analysis, it is possible to find the maximum power obtainable by first finding the optimal damping factor, ζ_{opt}.

This is given by the stationary point on $\frac{dP}{d\zeta}$, *i.e.*:

$$\zeta_{opt} = \frac{1}{2\omega_c}\sqrt{\omega_c^4 - 2\omega_c^2 + 1} \qquad (6)$$

(*Giving* $\zeta_{opt} = 0$ *for* $\omega_c = 1$)

The maximum power, P_{max}, which can be dissipated in the damper, and thus converted into electrical energy, is then obtained by substituting (eq.6) into (eq.5):

$$P_{max} = \frac{\omega_c^2 Y_0^2 m\omega^2}{\sqrt{\omega_c^4 - 2\omega_c^2 + 1}} \qquad (7)$$

The optimal value of ζ could violate constraints imposed by the system of which the most fundamental of these is the displacement limit, Z_l. The largest value of Z_l for currently reported MEMS micro-generators is 0.9*mm*. For given values of Y_o, ω_c and ζ, the unconstrained mass-to-frame amplitude, Z_0, is given by a rearrangement of (eq.3)

$$Z_0 = \frac{Y_0 \mu_c^{\,2}}{\sqrt{(1-\mu_c^{\,2}) + (2,\mu_c)^2}} \qquad (8)$$

If the optimal value of ζ means that the Z_l limits is exceeded, a larger ζ should be chosen so that the amplitude is reduced to just below the limit and an unclipped resonant cycle is achieved. Power as function of damping factor monotonically decreases each side of ζ_{opt} (for $\zeta_{opt} > 0$). Therefore the maximum (constrained optimal) power is achieved by operating as close to ζ_{opt} as possible while observing the displacement constraint. The constrained optimal damping factor, ζ_{optCZ}, is then given by a rearrangement of (eq.3):

$$\zeta_{optCZ} = \frac{1}{2\mu_c}\sqrt{\mu_c^{\,4}\left(\frac{Y_0}{Z_l}\right) - \left(1-\mu_c^{\,2}\right)^2} \qquad (9)$$

The power generated in this displacement on strained condition, P_{maxCZ}, is obtained by substituting(eq.9) into (eq.5):

$$P_{\max CZ} = Y_0^2 \mu^3 m \frac{1}{2\mu_c^2}\left(\frac{Z_t}{Y_0}\right)^2 \sqrt{\mu_c^4\left(\frac{Y_0}{Z_t}\right)^2 - \left(1-\mu_c^{\,2}\right)^2} \qquad (10)$$

Note that at resonance, the device is always displacement limited, because both the power, (given By (eq.5)), and the displacement, Z_0, tends to infinity for ζ tending to zero. Thus the power, P_{res}, That can be generated at resonance is obtained by setting $\omega_c = 1$ in (eq.10):

$$P_{res} = \frac{1}{2} Y_0^2 \mu^3 m \frac{Z_t}{Y_0} \qquad (11)$$

The surface plot for optimal power generation by an ideal VDRG is shown in Figure eq.5(a). As stated in the introduction, the power axis is normalized to $Y_0^{\,2}\omega^3 m$, and so is dimensionless. The height of the plot indicates the normalized power and the shading shows the damping factor, ζ, used at each point. This plot and equivalent plots for the VDRG assume that the damping factor is re-optimized for each operating point. This can be achieved by adjustment of the load electronics, where as variation of ω_n would require the spring constant to be varied. It was notedthat the curves of power against driving frequency shown by Williams, Yates *et al.* led them to an in accurate conclusion over optimal damping factors because in their plots, the driving frequency is swept as the independent variable, instead of the generator's resonant frequency. In Figure eq.5(a),and subsequent such plots, the shape is not subjected to this term because of the normalization, and thus the shape of the plot along the ω_c axis is the shape obtained when the resonant frequency,and not the drivingfrequency, is swept. The operating chart of Figure eq.5(b) shows which analytic expressions for power generation are valid under which circumstances. The regions are:

1. Device would generate more power if Z_0 could be increased beyond Z_l. Equation (eq.10) applies.
2. Device operating optimally for the value of ω_c. Equation (eq.7) applies.

3.2 Hysteretic Damping: In hysteretic damping, also called rate-independent or structural damping, energy is dissipated in a structure as it is loaded and unloaded, with the energy dissipated being equal to the loop integral of the area enclosed by the stress-strain curve . Glynne-Jones *et al.* have suggested hysteretic damping as an approximation for the type of damping provided by a piezoelectric generator, with a piezoelectric generator inherently working with the bending of a structure. Accurate modeling of

piezoelectric generator results in a much more complex form than can be modeled by simple damper. Hysteretic damping is often modeled with an equivalent viscous damper. If this approach is taken optimal forms of hysteretic damping produce the same normalized output power as for the VDRG as shown in Figure5(a).

3.3 Electromagnetic Implementation:

The damper in a VDRG will typically be formed of a moving magnet which produces a flux that links with a stationary coil of inductance, L, and resistance. The operating principle is that a voltage is induced in the coil due to the varying flux linkage caused by the movement of the magnet. The resultant currents causing forces which oppose the relative motion between the magnet and coil. In this analysis, the coil resistance has been lumped with the load resistance as R. The magnetic arrangement of Figure 6a is the most likely choice for an electromagnetic generator and has been used by Amirtharajah and Yates. The coil moves normally to the diverging field of a permanent magnet. For the arrangement of Figure 6a,Assuming the gradient of magnetic field, $\frac{dB}{dZ} = B'$, is constant across the plane of the coil ofarea A, the force on the coil can be worked out using the principle of virtual work as follows:

The rate of mechanical work being done in moving the coil, given by the product of the force on the coil multiplied by the velocity, is equal to the electrical power generated by the EMF, i.e. $f(t).\dot{z}(t) = i(t).e(t)$. The induced EMF is given by Faraday's law of induction and is $e(t)=\dot{z}(t)NB'A$. Consequently, the force on the coil is $f(t) = i(t)NB'A$ where N, A and B′ arenumber of turns on the coil, coil area and gradient of flux density respectively. In the Laplace domain, it means $F(s) = I(s)B'A$. If $I(s)$ is given by $E(s)/(R+sL)$, and $E(s) = sZ(s)NB'A$ then the force on the coil in the Laplace domain is given by $F(s) = \frac{(NAB')^2 sZ(s)}{(R+sL)}$

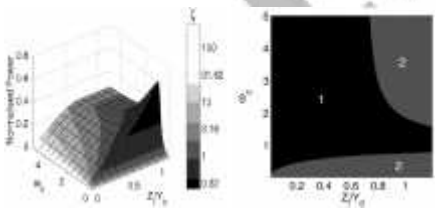

(a) Normalized power (b) Operating chart.
Figure5: VDRG idealized operation (no implementation limit).

Figure 6b shows a second possible linearized model, which is capable of providing a larger damping force than Figure6a because it contains a sharp transition from a uniform field region to a field-free region. This second arrangement is a popular model for analysis, but corresponds less well with realizations which have been reported. In this case, the damping force is given simply by the *BIL* force, *i.e.*$F(s) = \frac{(NBL)^2 sZ(s)}{(R+sL)}$

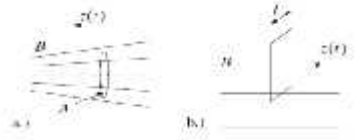

Figure6: Linearized magnetic models.

The differential equation of motion for these implementations is as equation.1, with the force on the moving magnet $f(t)$ taking the place of $D\dot{Z}(t)$. The displacement transfer function for the magnetic generator of Figure7, for the arrangement of Figure 6a, is obtained by taking the Laplace transform of this equation of motion and substituting in the expression for $F(s)$:

$$\frac{Z(s)}{Y(s)} = \frac{-s^2 m}{s^2 m + \frac{s(NAB')^2}{R+sL} + k} \qquad (12)$$

If the ωL product is small relative to R, then the system can be mapped exactly onto a velocity damped system with a damping coefficient

$\zeta = \omega_n (NB'A)^2 / 2\omega mR$. Amirtharajah makes this assumption by stating that the electrical pole is faster than the mechanical pole. However, for an optimized generator under certain conditions, this may not be the case. To achieve the large damping required at low $\frac{z_1}{y_0}$ ratios, the coil should have many turns and thus will have a large self-inductance. The resistance of the coil will increase if the conductor cross sectional area is not also increased, but the load resistance should be kept larger than the coil resistance to ensure high efficiency. The optimal damping factor may also require that the load impedance, R, is low. If ωL is not neglected then the modulus of the displacement transfer function is found by taking the magnitude of (eq.12):

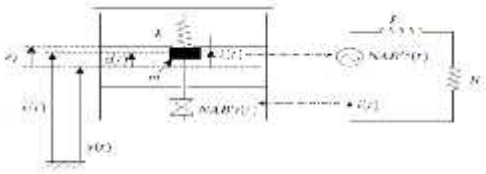

Figure7: Model of resonant electromagnetic generator.

$$\frac{Z_0}{Y_0} = \frac{m\mu^2\sqrt{R^2+\mu^2 L^2}}{\sqrt{m^2R^2(\mu_n^2-\mu^2)+\mu^2\left((NAB')^2+mL(\mu_n^2-\mu^2)\right)^2}} \qquad (13)$$

Thus, the maximum velocity V_0 of the relative motion is given by:

$$V_0 = \frac{Y_0 m\mu^3\sqrt{R^2+\mu^2L^2}}{\sqrt{m^2R^2(\mu_n^2-\mu^2)+\mu^2\left((NAB')^2+mL(\mu_n^2-\mu^2)\right)^2}} \quad (14)$$

The expression for the average power generated (*i.e.* dissipated in *R*)can then be found from1/2 (*peak voltage*)^2/*R*, where the peak voltage is given by $NA\,B'$ V_0:

$$P = \frac{m^2\mu^2\mu_c^2Y_0^2(NAB')^2R}{2R^2(1-\mu_c^2)^2m^2+2\mu^2\left(\left(\frac{NAB'\mu}{\mu_c}\right)^2+(1-\mu_c^2)mL\right)^2} \quad (15)$$

It should be noted that at resonance, (eq.15) reduces to that of a perfect velocity damper, because the inductor term is eliminated from the equation. However, at resonance, $\frac{z_o}{y_0}$is still dependent on *L*, as can be found by substituting $\omega=\omega_n$into (eq.13), giving

$$\frac{Z_0}{Y_0} = \frac{m\mu^2\sqrt{R^2+\mu^2L^2}}{\sqrt{(NAB')^2}} \quad (16)$$

Reducing the inductance of the coil reduces the relative displacement of the mass at resonance. This is helpful in two respects. In the displacement constrained case (Z_0= Z_l), for maximum realizable values ofB′, *N*, *A* and minimum realizable *R*, reducing *L* reduces the minimum $\frac{z_L}{y_0}$forwhich the device can operate. In the unconstrained case, the parasitic damping, which is amplitudedependent, will be reduced by reducing the displacement amplitude. Consequently, an optimal electro-magnetic design operating around resonance should have a minimum inductance, but still have the required flux linkage to obtain the required damping factor. This can be achieved either by tuning out the inductance with a capacitor, or by using a unity power-factor power converter connected to the coil.

Below resonance (*i.e.*, ω_c < 1) every term on the denominator of (eq.15) is positive and so in order to maximize power generation, the value of *L* should be as small as possible or tuned out. In order to gain some insight into why tuning out the inductance is often helpful to the operation of an electromagnetic generator (and to understand why in the unconstrained displacement case at resonance, the power generated is independent upon the presence of coil inductance) it is useful to consider the electrical equivalent circuit of the generator. Mappings from the mechanical to the electrical domain are given and a derivation of the equivalent circuit is also presented. The circuit is also shown here in Figure.8.

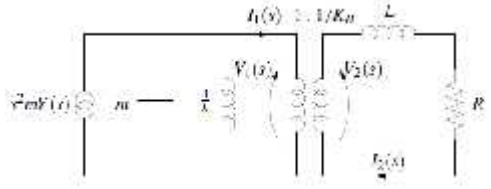

Figure.8: Equivalent circuit for an electromagnetic generator.

In Figure.8, the left hand side models the mechanical system and the right hand side the electrical system. The turn's ratio of the ideal transformer that links them is chosen as 1: $1/K_B$ because his allows the actual (un referred) load circuit elements to be attached directly to the mechanical system. K_B is the relation between the current in the coil and the damping force exerted on the mass, *i.e.* $f(t) = K_B X i_2(t)$ and is dependent upon the specific implementation of the generator. In this figure, $I_1(s)$ represents the force on the transducer, and $V_1(s)$ is the velocity of the transducer, mass and spring. These components are mechanically in parallel and consequently share velocity, which in this circuit is mapped to voltage. It can be seen from Figure.8 that at resonance, the power dissipated in the load resistance is independent of the load inductance because the series coil inductance and load resistance is fed directly from the current source (through the ideal transformer). $V_1(s)$ represents the velocity of the damper and thus it can be seen that reducing the coil reactance will, for a given value of the driving current source, reduce this maximum velocity and thus for sinusoidal motion will reduce the required mass-frame displacement.

3.4 Practical Constraints

There are practical limits on the realization of the velocity damper which will now be considered. These are:

- Maximum gradient and absolute value of magnetic field.
- Maximum coil area.
- Maximum number of coil turns achievable with an integrated inductor.
- Minimum combined impedance of the coil and power converter input stage.

If the inductor is tuned out of the circuit, or the value of ωL is negligible compared to *R*, then the system is a perfect velocity damper. Using the model of Figure6b, the damping factor is given by$\frac{(NBl)^2}{\omega_n 2mR}$. The four items listed above then place a limit on the

maximum realizable damping factor, ζ_{max}. An operating chart and optimal performance plot with constraints can now be plotted. These are shown in figures.9(a) and 9(b). As an example a flat, plated coil (Cu or Au) and a maximum coil area of 1 cm^2, for which a 10 turn coil of 1Ω resistance is reasonable, is assumed. Flux densities for permanent magnets do not generally exceed 1 T. Example values for mass and frequency of 0.5 g and 1.6 Hz respectively have been chosen.

The operating regions are as follows:

1. The device is unable to operate because the required ζ to meet the displacement constraint would be greater than the system can achieve.
2. The device operates at the displacement limit and (eq.10) applies.
3. The device operates optimally for the given value of ω_c and (eq.7) applies.
4. More power could be generated if the damping factor could be increased above the value of

ζ_{max} and (2.5) applies with $\zeta = \zeta_{max}$.

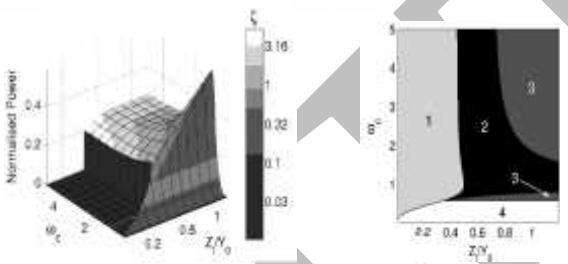

(a) Maximum normalized power. (b) Operating chart.

Figure.9: VDRG operation with ζ_{max} limit.

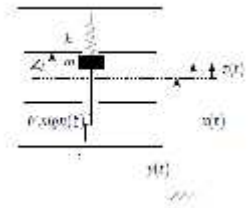

Figure.10: Model of CDRG.

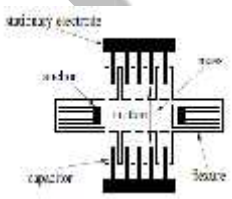

Figure.11: Possible MEMS

IMPLEMENTATION OF CDRG

IV. Coulomb-Damped Resonant Generators:

4.1 Ideal Case:

According to this analysis, the transfer function from frame motion to relative mass-to-frame motion is given by:

$$\frac{Z_0}{Y_0} = \mu_c^2 \left[\frac{1}{\left(1-\mu_c^2\right)^2} - \left(\frac{F}{mY_0\mu^2\mu_c} U \right)^2 \right]^{\frac{1}{2}} \qquad (17)$$

Where $U = \frac{\sin(\frac{\pi}{\omega_c})}{(1+\cos(\frac{\pi}{\omega_c}))}$ and F is the Coulomb force.

The energy dissipated is given by the force-distance product, and thus the power is:

$$P = \frac{4Y_0 F \mu \mu_c^2}{2®} \left[\frac{1}{\left(1-\mu_c^2\right)^2} - \left(\frac{F}{mY_0\mu^2\mu_c} U \right)^2 \right]^{\frac{1}{2}} \qquad (18)$$

This analysis can now be extended in the same way as for the VDRG. The Coulomb force which optimizes the power output, Fopt, is given by $\frac{dP}{dF} = 0$:

$$F_{opt} = \frac{Y_0\mu^2 m}{\sqrt{2}} \frac{\mu_c}{\left|\left(1-\mu_c^2\right)U\right|} \qquad (19)$$

The power, Pmax, dissipated in the Coulomb damper with the optimal force applied is then obtained by substituting (eq.19) into (eq.18):

$$P_{max} = \frac{\sqrt{2}}{®} Y_0^2 \mu^3 m \frac{\mu_c^3}{\left|\left(1-\mu_c^2\right)U\right|} \left[\frac{1}{(1-\mu_c^2)^2} - \frac{U}{(1-\mu_c^2)} \right]^{\frac{1}{2}} \qquad (20)$$

An important characteristic of the mass-frame displacement waveform is that a Coulomb-force can cause the relative motion between the proof-mass and the frame to reduce to zero for a period of time in which case the mass `sticks'. During this phase, no energy is generated.

The values taken by the Coulomb-force require some explanation. Sticking occurs when the mass has stopped relative to the frame and the absolute value of the Coulomb-force is larger than the absolute value of the sum of spring force and inertial force at that time. As soon as the mass starts to move in either relative direction, the Coulomb-force acts to oppose the motion and, during a sticking period, reverses the direction of the resulting relative acceleration. In a simulation this causes the mass to rapidly oscillate around a point which is stationary relative to the generator frame. As the simulation time-step is decreased the amplitude and period of this oscillation

Approach zero. This mode of operation is undesirable for a micro-generator as it makes the control and thus synchronization of the generator significantly more difficult. The requirement for nonstop motion is that the derivative of position is never zero within each half cycle. This is true if:

$$F < \frac{Y_0 \mu^2 m \mu_c^2}{\sqrt{\left(1+U^2\mu_c^2\right)\left(1-\mu_c^2\right)^2}} \qquad (21)$$

Note that this condition is only valid for ωc > 0:5. A method for calculating this limit is presented. It is possible for the value of optimal force calculated by (eq.19) to be greater than that allowed by (eq.21). This applies for ωc < 0:72. Under these conditions the optimal force is given by the limit of the inequality of (eq.21) and the power generated is obtained by substituting (eq.21) into (eq.18):

$$P_{\max} = \frac{2Y_0^2\mu^3\mu_c^4}{\sqrt{\left(1+U^2\mu_c^2\right)\left(1-\mu_c^2\right)}}\left[\frac{1}{(1-\mu_c^2)^2} - \frac{\mu_c U}{\sqrt{(1+U^2\mu_c^2)(1-\mu_c^2)^2}}\right] \qquad (22)$$

As for the VDRG, if the optimal force causes the displacement constraint to be exceeded, the force should be increased to preserve resonant motion. The optimal force that satisfies the displacement constraint, FoptCZ , is obtained by rearranging (eq.17):

$$F_{opt^{CZ}} = \frac{Y_0 \mu^2 m \mu_c}{|U|}\sqrt{\frac{1}{(1-\mu_c^2)^2} - \frac{1}{\mu_c^4}\left(\frac{Z_t}{Y_0}\right)^2} \qquad (23)$$

and thus the maximum power under a displacement constraint, PmaxCZ , is now obtained by substituting (eq.23) into (eq.18):

$$P_{\max^{CZ}} = \frac{2Y_0^2\mu_c m\mu^3}{|U|}\left(\frac{Z_t}{Y_0}\right)\sqrt{\frac{1}{(1-\mu_c^2)^2} - \frac{1}{\mu_c^4}\left(\frac{Z_t}{Y_0}\right)^2} \qquad (24)$$

It can be shown that at resonance (eq.24) reduces to (eq.11), i.e. optimal forms of the VDRG and the CDRG generate the same power at resonance. Figure 12(a) shows a surface plot of the power of the ideal Coulomb damper under optimized conditions. The power has been normalized using the same factor as for the VDRG. The Coulomb force can be normalized to Y0ω2m; this has been done for figures 12(a), 13(a) and 14(a). An operating chart is shown for the CDRG in Figure 12(b). The regions are as follows:

1. The device is not able to operate without stops in the motion because the force required to meet the displacement constraint (eq.23) is greater than that for which smooth motion is valid(eq.21).
2. For the given ω_c, more power would be generated if Z_l could be increased. (eq.24) applies.
3. The device operates optimally and (eq.20) and (eq.22) apply for ω_c > 0.72 and ω_c < 0.72respectively.

4.2 Practical Constraints:

For a CDRG operated at constant charge, the voltage across the capacitor plates increases linearly with separation. If the voltage reaches the limit for the load electronics the holding force must be increased (by increasing the charge) to reduce the range of travel sufficiently to keep the voltage within the limit. The optimal output power for the constant charge mode is shown in Figure 13(a). The corresponding operating regions are as follows (Figure 13(b)):

1. The device is unable to operate without stops in the motion.
2. The power is limited by Z_l and equation (.23) applies.
3. The device operates optimally and equations (.20) and (.22) apply for ω_c > 0.72 and ω_c < 0.72 respectively.

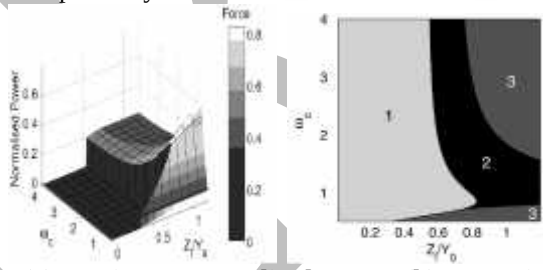

(a) Maximum normalised power. (b) Operating chart.

Figure .12: Idealised CDRG operation (no implementation constraint).

4. The power is constrained by maximum operating voltage. As an example a plate area of 1cm2, proof mass of 1g, ω =20π and Y0 = .1mm has been assumed. 400V has been chosen as a reasonable limit for integrating power semiconductors for which low power CMOS can be integrated on the same wafer. It is possible that a device could be limited by electric field strength but, in the constant charge mode, the maximum voltage occurs at the largest gap (the field strength is constant) and so the electric field strength is unlikely to be the limiting factor. However, higher field strengths can be supported in air over small distances, as described by Paschen's curve [206] and so it is possible that if pre-charged to too high voltage, breakdown of the dielectric between the plates could occur.

The optimal output power for constant voltage mode is shown in Figure.14 (a), and the corresponding operating regions in Figure (14(b)). This plot shows how the voltage constraint limits operation when the maximum available normalised force is, as an example, 0.68. This value has been chosen in order to clearly illustrate the effect of this limit:

1. The device is unable to operate without stops in the motion.
2. The power is limited by Z_l . Equation (.23) applies.

3. The device operates optimally. Equation (.20) applies for $\omega_c > 0.72$ and (.22) for $\omega_c < 0.72$.
4. More power would be generated if a greater Coulomb force could be realised.
5. The device is unable to operate: to meet the displacement constraint, the Coulomb force would have to be greater than that which can be provided by the system.

V. COULOMB-FORCE PARAMETRIC GENERATORS

5.1 Ideal Case:

The Coulomb-force parametric generator (CFPG), shown in Figure.15, is inherently non-linear in nature. The suspension is provided to guide the motion of the mass in a particular direction but is not designed to be resonant. If a spring is used at all it has a very small spring constant giving a resonant frequency very far below the normal operating frequency. The CFPG is controlled to only convert mechanical to electrical energy only when the generator frame is at maximum acceleration. For the case in which $\frac{Z_1}{Y_0}$ is small, this corresponds to the mass snapping back and forth between the end-stops at the peak of the frame acceleration cycle. If $\frac{Z_1}{Y_0}$ is large, the mass must be controlled to break away from the frame at an optimal acceleration and the energy must be extracted at the point of maximum separation. The snapping motion is illustrated in Figure .17. The proof mass is restrained by a holding force and work is only done when the acceleration is great enough to overcome this force. As the mass has to move some distance to do the work, the breakaway force cannot be the value of F_{max} in the input motion but must be some fraction, β, of it. Figure.16 shows a possible MEMS implementation. A variable-gap parallel-plate capacitor is formed between the BSOI device layer and a counter-electrode on the glass base plate, with the minimum gap being defined by a dielectric overlay on the counter-electrode. The suspension is

Designed to present very low resistance out of plane but be very stiff in the in-plane directions.

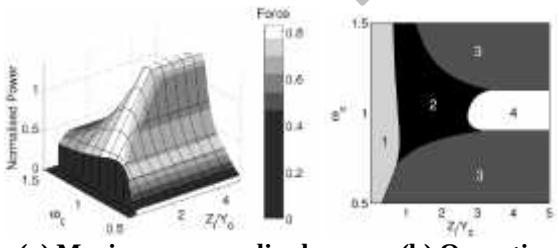

(a) Maximum normalised power. (b) Operating chart.

Figure.13: CDRG operation - perpendicular motion, constant Q.

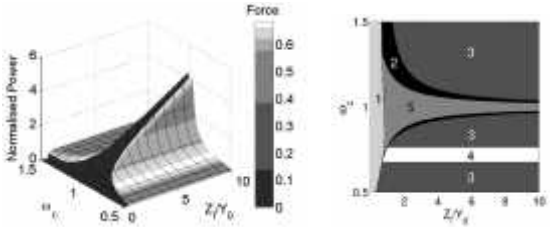

(a) Maximum normalised power. (b) Operating chart.

Figure.14: CDRG operation-sliding motion, constant V.

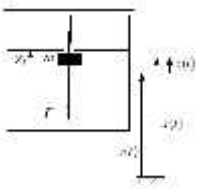

Figure.15.

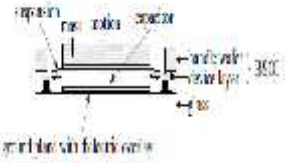

Figure.16:

Figure.15: Model of Coulomb-force parametric generator.

Figure.16: Possible MEMS implementation of CFPG

The energy generated by the parametric generator is given by the force-distance integral, which, if energy is extracted for both directions of motion, is:

$$P = 2\left(\frac{Z_0}{Y_0}\right)\frac{Y_0^2 \mu^3 m}{\text{®}} \qquad (25)$$

Again, optimising this generator requires the force-distance integral to be maximised. A possible method is to write the equations of motion and find the time at which the separation is maximum, at which point the maximum work will have been done. From this, the work done and its maximum with respect to the break-away force can be found. The acceleration of the moving mass during fight is constant in the inertial frame and so we obtain:

$$Z(t) - Z_t = Y_0 \cos(\sin^{-1}\ )[\mu t - \sin^{-1}\ ] - \frac{1}{2}\ Y_0[\mu t - \sin^{-1}\ ]^2 + \ Y_0 - Y_0 \sin \mu t \qquad (26)$$

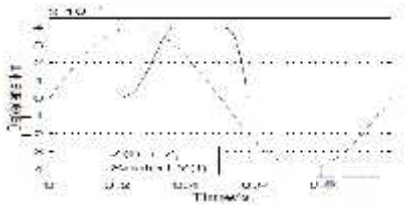

Figure.17: Optimal parametric motion for $\frac{Z_1}{Y_0} = 0.01$

The derivative of (eq.26) is similar to Kepler's equation and so has no closed form solution. However, we can observe that the value of *t* for

which $z(t)$ is maximum depends only on b and ω, and in fact can be written as $t_{max} = \frac{1}{\omega} f(\text{b})$.

Taking 2 Z_0 as the total displacement:

$$2Z_0 = Y_0 \cos(\sin^{-1}\ )[f(\ ) - \sin^{-1}\ ] - \frac{1}{2}\ Y_0[f(\ ) - \sin^{-1}\ ]^2 + \ Y_0 - Y_0 \sin f(\ ) \qquad (27)$$

Thus, β is solely a function of the ratio $\frac{Z_1}{Y_0}$ for sinusoidal input motion.

Time-domain simulations were run in Mat lab for the CFPG, varying β. These show that for small relative displacement limits, the optimal value of b for maximum power generation is that which allows the mass to just move the full distance, $2Z_1$. For values of $\frac{Z_1}{Y_0}$ above 0.566, b must be lowered more quickly than what is optimal for maximum power generation per stroke (where a stroke is defined as the movement of the mass in one direction to generate energy) because if power is extracted in both directions there is a need to change direction within half a cycle. For $\frac{Z_1}{Y_0}$ above 1.335, the need to allow for a change of direction causes the energy per stroke to be less than half that for single-sided operation (in which power is extracted in one direction only), and so single-sided operation gives greater total power. In the single-sided case the power generation stroke can last longer than half a cycle but the mass must return to its starting point within a full cycle to ensure periodic operation. This requirement limits the maximum value of b to 0.34 for $\frac{Z_1}{Y_0} > 1.16$. Sub-harmonic motion (*i.e.* only one power stroke every two or more cycles) has not been investigated, but would require a large value of $\frac{Z_1}{Y_0}$. It will be shown in Subsection 7.1 that the CFPG is a poor choice of generator under these circumstances.

The absolute limit of possible double-sided operation occurs when the proof mass is unable to run from side to side symmetrically, *i.e.* it reaches the other side of the device at the point at which it must break away again to return. This limit is found from (eq.26) by setting β = 0 and $t = \frac{2\pi}{\omega}$, giving $\frac{Z_1}{Y_0} \leq \frac{\pi}{2}$.

A plot of the optimal β values plotted against $\frac{Z_1}{Y_0}$ is shown in Figure.18. Figure.18 (a) shows optimal values for single-sided and double-sided operation, whilst 18(b) shows the optimal value and operating mode to use, assuming that the device can change between operating in double-sided or single-sided mode.

The maximum output power for the ideal parametric generator is shown in Figure.19(a). Although ω_c has no significance because there is no resonant frequency, graphs are still plotted against ω_c to ease comparison with the other generators. The corresponding operating chart is shown in Figure19(b). The regions are:

1. Optimal double-sided operation
2. β has to be reduced to allow double-sided operation but double-sided operation is still better than optimal single-sided operation.
3. Suboptimal single-sided operation (to allow periodic operation.)

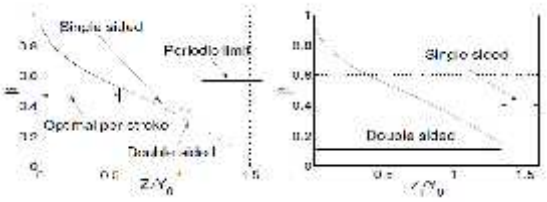

(a) Optimal β for single and double (b) β for optimal energy generation. Sided motion.
Figure.18: Optimal β values.

a. Practical Constraints:

As with the CDRG, the CFPG can use either sliding motion and constant voltage, or perpendicular motion and constant charge. For each case, the break-away force, and thus b, can be controlled by setting the initial voltage. For constant charge mode, the main constraint on optimal operation is likely to be the voltage capability of the output side power-processing circuitry. In this mode, the voltage increases from the start to the end of the cycle by the ratio of initial to final capacitance. For a comb style device, the limit on the applied voltage may restrict the Coulomb force to less than that needed for optimal operation. The power output for a constant charge mode CFPG is shown in Figure.20(a), and the corresponding operating chart is shown in figure.20(b). The operating regions are:

1. Optimal double-sided mode.
2. β reduced to enable double-sided operation.
3. This region is only present because of the voltage constraint. Double-sided operation with β reduced to stay within the voltage limit. The plot is for m=1 g, Y_0=0.5 mm, f=1 Hz, *Plate Area* = 1 cm^2, V_{limit} = 120 V. Although the output side power electronics could be designed to block more than 120*V*, this limit has been chosen to illustrate the effect more clearly.
4. This region is a constrained version of region 3 in the ideal case of Figure.19(b). Device in voltage limit for output-side electronics. Operation single-sided.

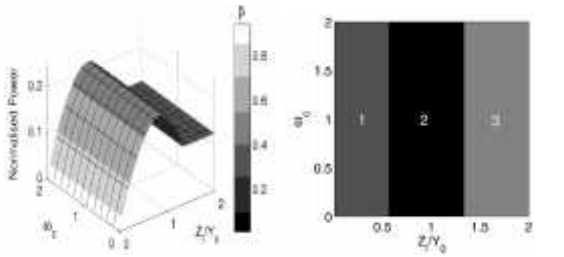

(a) Maximum normalised power. (b) Operating chart.

Figure.19: Idealised CFPG operation (no implementation constraint).

The power output for a constant voltage mode CFPG is shown in Figure.21 (a). The graph is plotted for the example of a maximum achievable β of 0.8. The corresponding operating chart is shown in Figure.21 (b). The operating regions are:

1. Device in voltage limit. β at the limit of 0.8.
2. Optimal double-sided operation - the device is operating optimally on each stroke.
3. β reduced to enable double-sided operation. Suboptimal double sided operation is still superior to optimal single sided operation in this region.
4. Suboptimal single-sided operation (to allow periodic operation).

VI. VELOCITY-DAMPED PARAMETRIC GENERATORS:

The velocity-damped parametric generator (VDPG) operates in a similar manner to the CFPG but with an energy extraction mechanism where the force characteristic of the damper is proportional to velocity rather than being a constant force opposing the motion (a Coulomb force). The operating mode is that the moving mass breaks away from the frame as soon as frame stops accelerating and starts decelerating and as a relative velocity occurs between the mass and the frame, energy is extracted through the damper. It will be shown in Subsection eq.7.1 that resonant generators are superior to non-resonant generators when the value of $\frac{z_l}{y_0} > 0.1$, and therefore

if a VDPG is superior in any mode of operation to any of the other types presented so far it will probably be when the ratio of $\frac{z_l}{y_0}$ is small. Velocity damping is most easily achieved using an electromagnetic transducer. However, it was shown in Figure.9 that an electromagnetic implementation of a micro-generator is not practical for values of $\frac{z_l}{y_0} <$ 0.5 (at low frequency) because the required damping force is not achievable.

The VDPG has therefore not been investigated further at this time, however if there was a means to make an effective velocity damper at a sufficiently small scale then this architecture may become attractive.

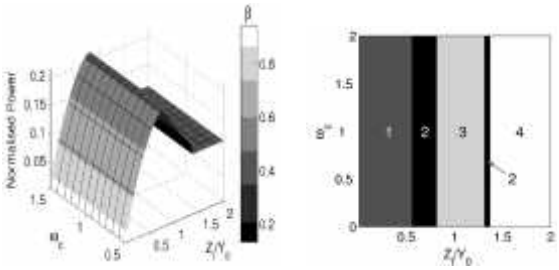

(a) Maximum normalised power. (b) Operating chart.

Figure.20: CFPG operation - perpendicular motion, constant Q (voltage limit).

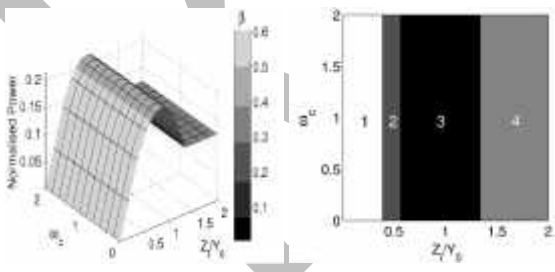

(a) Maximum normalised power. (b) Operating chart.

Figure.21: CFPG operation - perpendicular motion, constant V (force limit).

VII.DISCUSSION:

7.1 Comparison of Idealised Generator Types

Figure.22 compares the operation of the three generator architectures for a sinusoidal input. The dashed lines show the velocity, damping and displacement for a VDRG with values of m=1 g,k=80 N/m and D=0.475 Ns/m. The solid lines show the behaviour of the CDRG. An important characteristic of the mass-frame displacement waveform of the CDRG is that a Coulomb-force can cause the relative motion between the proof-mass and the frame to reduce to zero for a period of time, in which case the mass `sticks'. During this phase, no energy is generated. This is shown for two stops per half-cycle, with the solid line in Figure.22, where m=1 g, k=80 N/m, and F=0.95 mN. Sticking occurs when the mass has stopped relative to the frame and the absolute value of the Coulomb-force is larger than the absolute value of the sum of the spring force and the inertial force at that time. As soon as the mass starts to move, the Coulomb-force acts to oppose the motion and, during a sticking period, reverses the direction of the resulting relative acceleration. In simulation this causes the mass to oscillate around a stationary point relative to the generator frame. As the simulation time-step is decreased the amplitude

and period of this oscillation approach zero. Figure.22 shows the average force for the stationary periods in the cycle, as the results have been filtered to remove high frequency oscillation. In a practical CDRG, the capacitor being repeatedly charged and discharged would be lossy and consequently the device requires hysteresis around $\dot{z}(t)$ =0 in order to reduce the frequency of charging. Thus in a practical implementation, the mass would oscillate at reduced frequency but non-zero amplitude. The dotted line shows the operation of the CFPG for values of m=1 g and F=0.81 mN. Whilst it is useful to see the different modes of operation of the three generator architectures, the most important comparison between the generators is their achievable power density for given operating conditions. The graph of Figure.23 shows which optimised generator architecture can produce the most power as a function of operating condition. As can be seen, the CFPG is superior at low ratios of $\frac{Z_1}{Y_0}$, and for frequencies well below the resonant frequency of the resonant generators. The CDRG is superior below resonance (except for low $\frac{Z_1}{Y_0}$ values) and the VDRG is superior above resonance. The two give the same performance at resonance. The chart of Figure.24 shows a top-down view of Figure.23 and therefore reveals the best choice of generator (*i.e.* the architecture which achieves the highest power density) across the different normalised operating regions of $\frac{Z_1}{Y_0}$ and ω_c.

Taking the ratio of the maximum power output of the VDRG given by (eq.11) and the CFPG given by (eq.25), the following is obtained:

$$P_{CFPG} \Big/ P_{VDRG} = 4 \quad /® \qquad (28)$$

Where P_{CFPG} is the power output of a CFPG and P_{VDRG} is the power output of the VDRG.
This indicates that the CFPG can generate more power than resonant generators where the optimal β value is above $\pi/4$; this corresponds to a displacement limit $\frac{Z_1}{Y_0}$ of 0.107.

Applications for micro-power generators fall into two main categories: devices powered by human body motion and those powered by vibration of machinery. Body motion (of limbs or the cardiovascular system) is of low frequency and relatively high amplitude compared to the dimensions of reported generators whereas the vibrations of machinery are generally of high frequency and low amplitude. Thus, the parametric generator is suitable for generating power from the human body, whilst resonant generators are appropriate for generating power from machinery (at least for a source of narrow frequency range).

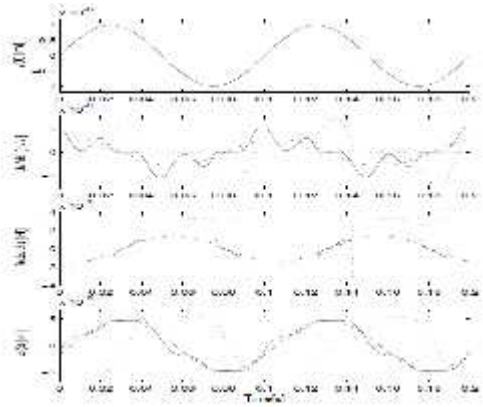

Figure.22: Comparison of the operation of the three generator architectures. Dashed line is the VDRG, solid line the CDRG, and dotted the CFPG. $\pm Z_1$ is shown as dashed straight lines.

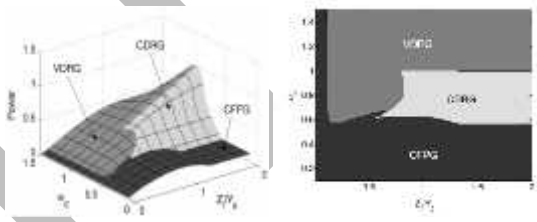

Fig.23 Fig.24

Figure.23: Generator architecture comparison.
Figure.24: Best architecture choice under the different normalised operating conditions.

a. Parasitic Damping:

Parasitic damping effects, such as air resistance or hysteresis loss in the suspension, are difficult to estimate in general terms because they are dependent upon materials, structure, and maximum displacement. Consequently, the above analysis has not included parasitic damping. However, the limits on the absolute validity of the results will now be discussed. Williams *et al.* state that for their generator, the measured parasitic damping factor, ζ_p, due to the air and spring hysteresis is of the order of 0.0037 and the measured value for their device operated in vacuum is 0.0023. Optimal operation of this device (a VDRG) requires an electrical damping factor $\zeta_e = \frac{Y_0}{2Z_1}$ (equation.3 with ω_c= 1.) For electrical damping to dominate in the vacuum case (e.g. $\zeta_e \geq 10\zeta_p$) requires $\frac{Z_1}{Y_0} < 20$. The range of reported values of Z_1 and Y_0 suggest that parasitic damping may be significant in some situations if the value of the parasitic damping reported by Williams *et al.* is typical. Roundy *et al.* look in some detail at the effect of parasitic damping of electrostatic generators. For an optimised generator, the parasitic damping could

be significantly reduced over the design. For example, Nguyen states that air damping is the dominant parasitic for micro-mechanical resonators for Q of up to 50,000 and beyond this hysteretic damping within the spring material is the dominant factor. Elimination of air damping by e.g vacuum packaging in this case would therefore yield a residual damping factor of $2X10^{-5}$. The discrepancy between the maximum Q values reported by Nguyen and Williams are probably because of the differences in materials used. Nguyen's resonators use silicon and the micro-generator of Williams uses a polyimide suspension, which is a much more lossy material.

The power generated by a resonant VDRG with parasitic damping can be written, as:

$$P = \frac{\zeta_e \mu_c^3 Y_0^2 \mu^3 m}{\left[1-\omega_c^2\right]^2 + \left[2(\zeta_t+\zeta_e)\omega_c\right]^2} \quad (29)$$

Where $\zeta_t = \zeta_e - \zeta_p$. Should the parasitic damping be significant, the electrical damping factor should be re-optimised. For a velocity damper, this optimal ζ_e is again given by the stationary point on $\frac{dP}{d\zeta_e}$:

$$\zeta_e = \frac{1}{2\mu_c}\sqrt{1-2\mu_c^2+\mu_c^4+4\mu_c^4\zeta_p^2} \quad (30)$$

An equivalent optimal damping factor can be obtained for the Coulomb damped case in the same fashion. Levitan described an analytical solution to the support excited system with combined Coulomb and viscous damping. The analysis will not be presented here, but could perhaps be used to find an optimal operating condition where both damping mechanisms are present.

7.3 Vibration Source Limitations:

Due to the small mass of a micro-generator, and the relatively small amount of power that is harvested, micro-generators are likely to have little effect on a vibration source to which they are attached. This effect can be quantified by considering the source to have an internal damper analogous to the output impedance of a voltage source. Modelling such a system suggests that if the power extracted by the micro-generator is more than 1% of the maximum output of the source, the effect of the source limitation on performance becomes significant.

VIII. GENERATOR EFFECTIVENESS:

It has not until now been possible to quantify the success of the designs of micro-generators because an adequate measure of performance had not been identified. Such a quantity, which allows the performance of micro-generator designs to be quantified and compared, was developed in the course of this work and is now described.

The most important performance metric for a micro-generator is the proportion of the theoretical maximum power density that is achieved by the device, for the given device volume and vibration source from which the device is powered. This performance measure will be referred to as the *effectiveness* of the generator.

In this work, generator effectiveness is defined as the product of two terms:

$$Effectiveness = \frac{P_{out}}{P_{opp}} \quad (31)$$

$$= \eta_{mech} \times \eta = \frac{P_{coupled}}{P_{opp}} \times \frac{P_{out}}{P_{coupled}} \quad (32)$$

where:
P_{out} is the useful output power after processing,
$P_{coupled}$ is the mechanical power coupled into the generator,
P_{opp} is the opportunity power, or the maximum power that could have been coupled using a generator operating optimally,
η_{mech} is the mechanical coupling effectiveness and
η is the generator efficiency.

The mechanical coupling effectiveness of a generator is thus a measure of the proportion of the energy that is dissipated in the damper in the mechanical generator model, as a function of the total amount of energy that could have been dissipated in the damper if all the generator parameters had been optimally set for the given vibration source from which the device is powered. This is a measure of an opportunity power and thus the term is referred to as effectiveness rather than efficiency (a coupling effectiveness lower than 1 does not occur because of energy wasted as a dissipation of heat, for example). The efficiency of the generator is a then the fraction of that coupled energy which is converted in to a useful electrical form for the load electronics, with losses occurring due to inefficiencies in the power processing.

The work in this chapter has established the ultimate performance limits for three different architectures of micro-generator, under all operating conditions, and this allows the effectiveness of the reported micro-generators to be calculated.

8.1 The Effectiveness of Published Work:

Where the relevant information is available (*i.e.* Y_0,ω, Z_l , m and device volume), the performance of some previously reported generators can now be discussed.

- The vast majority of the reported devices perform with very low effectiveness values, many being less, and some being significantly less, than 1%. This can be attributed in many cases to a mixture of parasitic damping and a non-optimal choice of damping force. As an example, the damping force used by Meninger *et al.* was severely limited because the associated generator electronics was fabricated in low voltage CMOS.
- In all cases, the effectiveness of the generator for the reported parameters is less than that for the device built into a cube of the same volume. A cube is actually a relatively poor shape of micro-generator, because the axis in which a mass, occupying half the volume, can move is shorter than for any rectangular shape. This suggests that the authors may have been limited in the geometry of their generators due to practical constraints.
- The measured values tend to be lower than predicted by the models.
- Roundy *et al.* present the generator with the highest effectiveness of any of the measured values.
- Tom Sterken reports a power output figure which gives effectiveness significantly greater than 100% from one of his electrostatic models. This is possibly because Sterken quotes power outputs from a model of the generator linearised around the equilibrium point. At resonance, the relative displacement of the proof-mass is significant and it is possible that the linearization is no longer valid.
- Yates *et al.* report effectiveness values greater than 100% for their electromagnetic generator model. As they use the simple equation for power output as for a VDRG operating at the resonant frequency, it is likely that this is a numeral error on their part and their effectiveness value for their parameters should be 100%.
- There is no obvious trend as to which type of generator implementation has proved most successful in the literature, as all methods have yielded some implementations with very low effectiveness values and some higher. However, it should be noted that whilst a fabricated piezoelectric generator has been reported by Roundy *et al.* with an effectiveness of 16.8% and an electrostatic generator with a measured power output reported by Miyazaki *et al.* achieves an effectiveness of 12.4%, the highest effectiveness figure achieved from a fabricated electromagnetic generator is 1.1%, by El-Hami *et al.*

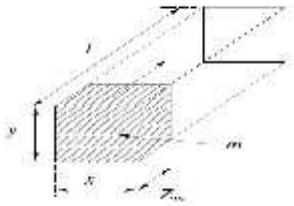

Figure.25: Mass constrained to move in a volume.

8.2 Expected Maximum Power Densities:

The ultimate limiting factor for an inertial micro-generator is its size which limits both the mass and the travel that can be used (Z_l). Since, for a resonant generator operating at resonance, or a CFPG operating when $Z = Z_l$ with constant β, the power is linearly proportional to both m and to Z_l, the power is maximised for a mass taking up half the device volume. This can be justified as follows with reference to Figure.25.

In the direction of motion, the overall device dimension, l, must be divided between the range of internal travel, $2Z_l$, and the dimension of the mass in that direction, Z_m. Since the output power is proportional to the product of mass and $2Z_l$ (for a given operating condition), power will be maximised for $Z_l = Z_m/2$, *i.e.* for the mass taking up half the space. Power will now be proportional to l^2, and to the other two spatial dimensions x and y. This suggests that micro-generator power output (at resonance or when $Z = Z_l$ for the CFPG) is proportional to *volume* $^{4/3}$(assuming uniform scaling in each spatial dimension).

The effectiveness figures discussed so far are the limits of the power that can be coupled in to the damper. However, the electrical power which can be generated will be some proportion of that coupled power because of various losses. These losses include:

- Parasitic damping will reduce the maximum electrical power as discussed above.
- Charge will leak from the plates of an electrostatic generator during the generation cycle because of the non-zero conductance between them. This reduces the Coulomb-force, and thus the power generated.
- Some power will be consumed by the control electronics needed by the generator.
- There will be electrical conduction and switching losses.

To estimate the maximum power available from a MEMS generator, the following data are taken. The highest density r of a MEMS material is that of gold, which is the example taken here, a generator

effectiveness of 100% is the target and a volume of 1 cm3 is realisable.

For a human powered application (with movements at 1 Hz and 5 mm amplitude) a power density of $4\mu W/cm^3$, could be available using a parametric generator. This will be sufficient for some autonomous sensor applications.

For a machine powered application (with vibrations of, for example, 2nm at 2500Hz), a resonant generator could yield a power density close to $9.6mW/cm^3$.

IX. CONCLUSIONS

In this work, analysis of three micro-generator architectures has been presented with a view to understanding the relative merits of each, and in order to find optimal architectures for maximal power generation under the different operating constraints of displacement and normalised frequency. Analysis has been verified by time-domain simulation. It has been shown that under operating conditions of known $\frac{Z_l}{Y_0}$ and $\frac{\omega}{\omega_n}$ ratios, the expressions for the power generated for all architectures can be normalised to $Y_0^2\,\omega^3 m$. For ideal implementations, the following conclusions hold:

- The CFPG produces the most power where $\frac{Z_l}{Y_0} < 0.1$
- The VDRG is superior above the resonant frequency when $\frac{Z_l}{Y_0} > 0.1$
- The CDRG is superior below but near the resonant frequency when $\frac{Z_l}{Y_0} > 0.1$
- Generators only benefit from operating at or near resonance when $Z_l > Y_0$.
- It is not possible to operate a CDRG at low $\frac{Z_l}{Y_0}$ ratios and maintain smooth motion of the proof mass, making the generator control and synchronisation difficult.

Additional conclusions can be drawn when practical implementation issues are taken into account:

- It is not possible to operate the VDRG for small $\frac{Z_l}{Y_0}$ ratios. At some value of, the required damping factor will become unrealisable due to limits on minimum coil and load impedance and maximum achievable magnetic field strength.
- At the resonant frequency, the coil inductance of the resonant electromagnetic generators has no effect upon performance, because the system simplifies exactly to a perfect VDRG.

Some basic design steps for the micro-generator designer can now be formulated:

1. Make the volume of the device as large as possible and make the axis in which the mass moves as long as possible within the constraints of the application. This establishes the value of Z_l.
2. Choose the generator architecture which gives the highest power density for the values of $\frac{Z_l}{Y_0}$ and $\frac{\omega}{\omega_n}$ from Figure.24.
3. Choose a suitable implementation method for that architecture taking into account practical limitations of the technology.

X. ACKNOWLEDGEMENTS

We thank Professor **Dr. B.Raghu kumar** for their constant encouragement and support.

We are grateful to professor **Dr. Y. V. S. S. S. V. Prasad Rao** and Professor **Dr. CH. Sanjay** for many helpful and stimulating discussions.

XI. BIBLIOGRAPHY

[1]. D.Wanless, *.Securing Our Future Health: Taking a Long Term View,. HM Treasury, U.K., Tech. Rep., April 2002.*

[2]. A. Flowerday and R. Smith, *.Lessons Learnt from Long-Term Chronic Condition Monitoring,. in 1st International Workshop on Wearable and Implantable Body Sensor Networks Proceedings, Imperial College London, U.K., April 2004*.

[3]. P. Needham and L. Gamlyn, *Arrhythmia Analysis in the Community. in International Workshop on Wearable and Implantable Body Sensor Networks Proceedings, Imperial College London, U.K., April 2004.*

[4]. L. Gamlyn, P. Needham, S. M. Sopher, and T. J. Harris, *.The Development of a Neural Network-Based Ambulatory ECG Monitor,. Neural Computing and Applications, vol. 41, no. 4, pp. 273.278, April 1999.*

[5]. A. Heller, *Drug Delivering Integrated The raputic Systems. in 2nd International Workshop on Wearable and Implantable Body Sensor Networks, Imperial College London, South Kensington, London, UK, April 2005, pp. 6.11.*

[6]. B. B. Owens, *Batteries for Implantable Biomedical Devices. 233 Spring Street, New York, N. Y.: Plenum Press, 1986*.

[7]. S. Roundy, D. Steingart, L. Frechette, P. Wright, and J. Rabaey, *.Power Sources for Wireless Sensor Nodes,. Lecture Notes in Computer Science, vol. 2920 / 2004, pp. 1.17, January 2004.*

